EFFECT OF LEADING-EDGE GEOMETRY ON BOUNDARY-LAYER RECEPTIVITY TO FREESTREAM SOUND

N92-14970

N Lin[1], *H L Reed and W S Saric*

Arizona State University

Tempe, Arizona 85287-6106

ABSTRACT

The receptivity to freestream sound of the laminar boundary layer over a semi-infinite flat plate with an elliptic leading edge is simulated numerically. The incompressible flow past the flat plate is computed by solving the full Navier-Stokes equations in general curvilinear coordinates. A finite-difference method which is second-order accurate in space and time is used. Spatial and temporal developments of the the Tollmien-Schlichting wave in the boundary layer, due to small-amplitude time-harmonic oscillations of the freestream velocity that closely simulate a sound wave travelling parallel to the plate, are observed. The effect of leading-edge curvature is studied by varying the aspect ratio of the ellipse. Boundary layer over the flat plate with a sharper leading edge is found to be less receptive. The relative contribution of the discontinuity in curvature at the ellipse-flat-plate juncture to receptivity is investigated by smoothing the juncture with a polynomial. Continuous curvature leads to less receptivity. A new geometry of the leading edge, a modified super-ellipse, which provides continuous curvature at the juncture with the flat plate, is used to study the effect of continuous curvature and inherent pressure gradient on receptivity.

Nomenclature

U	freestream velocity
L	half-thickness of the flat plate, minor radius of the ellipse
r_n	leading-edge nose radius
ν	kinematic viscosity
Re	Reynolds number, UL/ν
Ω	frequency of oscillations
F	non-dimensional frequency parameter, $\Omega\nu/U^2$

S_n Strouhal number based on nose radius, $\Omega r_n / U$

AR   aspect ratio of the ellipse

a   amplitude of freestream oscillations

MSE   modified super-ellipse

TS   Tollmien-Schlichting

K   surface curvature

x,y   Cartesian coordinates parallel and normal to the flat plate, respectively

u'   streamwise perturbation velocity, in x-direction

v'   normal perturbation velocity, in y-direction

ω' perturbation vorticity

Cp   steady-state pressure coefficient

1. Introduction

Receptivity, the process by which external disturbances lead to instabilities in shear flows, plays a vital role in the transition from laminar to turbulent flow. The importance of receptivity in prediction, modelling and control of transition has been recognized [Morkovin (1978), Reshotko (1984)] and can not be overemphasized. Substantial progress has been made in investigating receptivity of boundary layers. Discussions of recent developments in boundary-layer receptivity theory may be found in Goldstein and Hultgren(1989) and Kerschen (1990). A detailed review of some experiments on receptivity are presented in Nishioka and Morkovin (1986).

In the prediction of boundary-layer receptivity to freestream long-wavelength disturbances, theoretical investigations based on high-Reynolds-number asymptotic methods have identified that the conversion of freestream disturbances to TS instability waves takes place in the boundary layer where the mean flow exhibits rapid local variations in the streamwise direction [Kerschen (1990,1991), Goldstein (1983,1985)]. The discussions here concentrate on receptivity to sound in the leading-edge region.

A few experiments, using flat plates with elliptic leading edges, have been done on boundary-layer receptivity to freestream sound. In Leehey and Shapiro (1980) and Leehey et al. (1984) a leading edge with AR=6 was used. Acoustic receptivity for their flat plate was reduced from order one to essentially nothing after tipping the plate to obtain a zero mean-pressure gradient [Leehey et al. (1984)]. Results of Wlezien and Parekh (1990) and Parekh et al. (1991), using AR=6 and AR=24 (on a solid plate) indicate that the flat plate with a sharper leading edge is less receptive to a plane sound wave. In their

experiments mean-pressure gradients are effectively zero and junctures between the leading edge and the flat plate are smoothed by a filler.

In terms of the computational modelling of the boundary-layer receptivity to long-wavelength acoustic waves, Kachanov et al. (1978) solved the incompressible flow over an infinitely thin flat plate, using the Navier-Stokes equations linearized for small disturbances. A freestream vortical disturbance and a transverse acoustic wave across the leading edge were considered. Murdock (1980) studied the receptivity to a plane parallel sound wave of an incompressible boundary layer over a flat plate with no thickness, and boundary layer over parabolic bodies (Murdock 1981). Receptivity was found to occur near the leading edge. A sharper leading edge (smaller nose radius, r_n) was reported to be more receptive. Hammerton & Kerschen (1991) found that the effect of nose bluntness was to decrease leading-edge receptivity for a plane acoustic wave propagating parallel to a parabolic body. It should be noted that these bodies have favorable pressure gradients everywhere. Gatski and Grosch (1987) solved the full incompressible Navier-Stokes equations for flow over an infinitely thin, semi-infinite flat plate. No clear development of the TS wave due to freestream oscillations was reported.

These results from experiments, computations and theories indicate that differences in not only parameters such as F and Rc, but also details of leading-edge curvature, local and freestream steady/unsteady pressure gradients can affect receptivity greatly. In an attempt to investigate boundary-layer receptivity mechanisms to different freestream disturbances, a numerical code has been developed to compute the unsteady incompressible flow over a semi-infinite flat plate with an elliptic leading edge solving the full unsteady Navier-Stokes equations (Lin 1989). The use of a body-fitted curvilinear grid in this work enables us to perform direct simulations with a variety of leading-edge geometries.

2. Numerical Formulation

The governing equations are the two-dimensional unsteady incompressible Navier-Stokes equations with vorticity and stream function as dependent variables. A C-type orthogonal grid is generated around the leading edge and the flat plate (Fig. 1). The boundary conditions are the usual no-slip and no-penetration conditions at the wall, inviscid freestream velocities at the farfield boundary, and numerical boundary conditions downstream (Fasel 1976). The equations and boundary conditions are written in general curvilinear coordinates and discretized in space and time, using second-order accurate finite

differences. The resulting system of equations is solved using a modified strongly implicit procedure of Schneider and Zedan (1981). Further details of the numerical formulation may be found in Lin (1989).

First, a basic-state solution is computed by solving the governing equations for steady, incompressible flow with a uniform freestream, using a transient approach and spatially varying time steps. Then the steady flow is disturbed by applying forced perturbations about the steady basic flow at the freestream as unsteady boundary conditions. The resulting unsteady flow and the temporal and spatial development of the perturbations are calculated by solving the unsteady governing equations time accurately. Here, time-harmonic small-amplitude oscillations of the freestream streamwise velocity about the steady flow, which closely simulate a sound wave travelling parallel to the flat plate in the incompressible limit, are used as freestream perturbations.

3. Results and Discussions

3.1. Steady-state solutions

Steady-state solutions are obtained for three different values of the aspect ratio (AR) of the semi-ellipse, i.e. AR =3, 6 and 9. In all cases, the Reynolds number, based on half-thickness of the flat plate or the minor radius of the semi-ellipse L and the freestream velocity U, is chosen to be 2400. In modelling the semi-infinite flat plate the downstream computational boundary is located such that the branch I of the neutral stability curve for Blasius flow (according to linear parallel theory) is well within the computational domain. The farfield computational boundary is located at about 25 to 30 Blasius-boundary-layer thicknesses at the downstream region. The grid-point distribution in the streamwise direction is determined not only to ensure high resolution of the leading-edge region where the curvature is changing rapidly, and at the ellipse-flat-plate juncture, but also to have at least 10 to 20 grid points in one expected TS wavelength for unsteady calculations. The stretching in the normal direction is done to pack more grid points near the wall to resolve the boundary layer and the Stokes viscous layer of the unsteady solution. Numerical studies have been made to insure the adequacy of grid resolution and computational boundary locations.

Typical steady-state solutions are presented in Figures 2 and 3. The wall vorticity (Fig. 2) differs appreciably from that of the Blasius solution near the leading edge. The sharper leading edges exhibit a peak vorticity closer to the singular behavior of the Blasius vorticity,

as expected. Velocity vector profiles accordingly differ from Blasius profiles, having overshoots above the freestream velocity at the leading-edge region. The surface pressure coefficient distributions (Fig. 3) of the sharper leading edges have smaller pressure minima after acceleration around the leading edge, hence smaller magnitudes of adverse pressure gradient in the pressure-recovery region. After this recovery, the pressure coefficient is very close to the inviscid solution, with a very small and almost constant adverse pressure gradient downstream. The square of the displacement thickness varies linearly with x, after some distance from the leading edge (Lin et al.1991). The virtual leading edges are located upstream of the actual ones, due to rapid thickening of the boundary layer in the pressure-recovery region.

3.2. Unsteady solutions

Unsteady calculations are carried out at different values of the nondimensional frequency parameter, i.e. $F=333\times10^{-6}$ and 230×10^{-6} for a leading edge with AR=3 (Lin 1989) and $F=230\times10^{-6}$. and 110×10^{-6} for AR=6 and 9 (Lin et al. 1991). The amplitude of the freestream oscillations (or the amplitude of the sound wave, a) used in these calculations is either $10^{-4}U$ or $2\times10^{-4}U$. Detailed discussions of the temporal and spatial development of perturbations in the boundary layer are given in the above references. After the theoretical Stokes-wave solution is subtracted from the total perturbation obtained from the Navier-Stokes solution, the amplitude profiles of the remaining disturbance can be calculated. These profiles are found to gradually develop into typical TS-wave amplitude profiles (Fig. 4) after some distance from the ellipse-flat-plate juncture and are zero after the TS wavefront.

The streamwise variation of Fourier amplitude and phase (obtained by performing temporal Fast Fourier Transforms) for the u' disturbance velocities (along the j=9 grid line) are shown in Figures 5 and 6. These amplitude and phase variations are typical of a TS wave linearly superposed on a long-wavelength disturbance (Stokes wave). In the flat-plate region, the v' component of the disturbance response is mostly contributed by the TS wave. Therefore wavenumber information of the TS wave present in unsteady solutions is extracted by differentiating the Fourier phase of the v' in the streamwise direction. These wavenumbers are shown together with wavenumbers obtained by linear stability analysis of the Navier-Stokes basic-state solution in Figure 7 . The locations of the branch I neutral stability curve predicted by the unsteady Navier-Stokes solution and by the linear stability analysis of the Navier-Stokes basic-state solution are close and occur

well upstream of the branch I based on the Blasius boundary layer. In Figure 8, a typical result of grid-refinement studies is shown. It is clear that 200x80 grid points are adequate (for $F=230 \times 10^{-6}$) to get accurate solutions in the leading-edge region and further downstream except the TS-wavefront region. A finer grid than 280x90 would be required to resolve smaller scales present in the leading wave-packet, which is beyond the scope of this work.

3.3. Effect of leading-edge geometry

The effect of leading-edge curvature on receptivity is investigated by varying the AR of the ellipse while keeping the half-thickness L (hence Re) the same. The amplitude of the TS wave is smaller for sharper leading edges. This can be seen clearly in surface plots of instantaneous streamwise disturbance velocity, u', after 4 cycles of forcing and after subtracting the Stokes wave (Fig. 9 and 10). The magnitude of receptivity, as defined by the maximum (in y) amplitude of u' (of the TS wave only) in the boundary layer to the amplitude of the freestream sound, a, is found to be about 0.8, i.e. order one, for the AR=3 leading edge at $F=230 \times 10^{-6}$, while the magnitude of receptivity is found to be of order (10^{-1}) for the AR=9 leading edge. For the AR=6 plate, the magnitude is of the same order but approximately twice as large as the AR=9 plate. A sharper leading edge has a larger curvature at the nose, has a smaller (in magnitude) local adverse pressure gradient in the leading-edge region, and also has a smaller magnitude of discontinuity in curvature at the ellipse-flat-plate juncture. It is a combination of these factors that may contribute to reduced receptivity.

As for the effect of frequency parameter F (for the same AR), a lower value of F is found to give a larger amplitude of u' near the juncture. This trend is in qualitative agreement with the theory of Goldstein (1985, 1989). It should be mentioned that for a fixed nose radius r_n, lower F means lower Strouhal number, S_n, hence the contribution from the nose bluntness should be higher according to results of Hammerton and Kerschen (1991) based on parabolic bodies. Farther downstream, the TS wave amplitude is smaller for a lower F since damping rates before the first neutral-stability point are stronger.

The wavelength conversion process necessary for receptivity to freestream long-wavelength disturbances is illustrated in plots of instantaneous disturbance streamlines (Fig.11 and 12). A disturbance structure which has a larger length scale than the TS wavelength and extends well beyond the boundary layer in the normal direction can be

observed at the leading edge. This structure has about twice the TS wavelength in the case of $F=110 \times 10^{-6}$ (see also Fig. 6). At the edge of the steady boundary layer, it can be considered as unsteady pressure gradient $A(x)$ input to the boundary layer, in light of discussions given by Nishioka and Morkovin (1986). One may relate it to eigen-solutions of the unsteady boundary layer as described in Goldstein (1983).

The asymptotic theories of Goldstein and Hultgren (1989), in comparison with the experiments of Leehey and Shapiro (1980) predicted that discontinuity in curvature at the juncture contributes more to order-one receptivity, while the disturbances incepted due to leading-edge adjustment of the boundary layer (Goldstein 1983) have a much smaller contribution due to their rapid decay. To determine the effect of the discontinuity in surface curvature, a portion of the surface at the juncture region of the AR=6 leading edge is replaced by a polynomial, making the curvature continuous everywhere. Figure 13 illustrates the surface-curvature variation before and after this smoothing. The inherent change in the pressure gradient due to smoothing along the surface is small and an enlarged view of the pressure gradient near the juncture is given in Figure 14. Then steady and unsteady results are obtained at $F=230 \times 10^{-6}$, using the same grid resolution and time-step size. The two solutions obtained with continuous and discontinuous curvature are compared in Figure 15. It is clear that discontinuous curvature enhances receptivity.

In order to investigate the effect of continuous curvature and inherent pressure gradient of the leading-edge, a new leading-edge geometry based on a super-ellipse is considered. The shape of this modified super-ellipse (MSE) is given by the following formula.

$$[\, 1 - x/(AR\ L)\,]^{m(x)} + [y/L]^{n} = 1, \qquad 0 < x/L < AR$$

$$m(x) = 2 + [\,x/(AR\ L\,)\,]^{2} \text{ and } n = 2$$

For a usual super-ellipse, both m and n are constants. Several leading-edge geometries can be designed by using different constant values for m and n. These super-ellipses will have the advantage of a continuous curvature (zero) at the juncture with the flat plate as long as m is greater than or equal to 3 at x/L=AR. The MSE, with m(x) given above, has the further advantage of having a nose radius and geometry (hence a pressure distribution) close to that of an ordinary ellipse with m=2 and n=2 (Fig. 16).

Variation of steady wall pressure gradient for the AR=6 MSE is given in Figure 14. See Figure 12.b for contours of instantaneous disturbance streamlines. Plots of instantaneous wall disturbance vorticity at $F=230 \times 10^{-6}$ (Fig. 17) show that the MSE geometry is as

receptive as an ellipse (with a discontinuous curvature) of the same AR. The MSE has a steeper adverse pressure gradient near the juncture, although the curvature is continuous. This indicates that a rapid (continuous) change in this adverse pressure gradient region is as important as the discontinuity in curvature.

Further calculations at different Re, F, AR and different leading-edge geometries, comparisons with results of different numerical schemes and grid generation methods, local comparisons with available theories and direct comparisons with experimental results, should be carried out in the near future.

4. Conclusions

The receptivity of the laminar boundary layer over a semi-infinite flat plate at the leading-edge region is investigated by direct numerical solution of the full Navier-Stokes equations. The leading-edge curvature and finite thickness of the flat plate are included by using body-fitted coordinates.

We are able to observe both temporal and spatial initial developments of the TS wave in the boundary layer due to time-harmonic oscillations of the freestream streamwise velocity. The receptivity occurs in the leading-edge region where rapid adjustments of the basic flow exist. In this region the variation of curvature, the adjustment of the growing boundary layer, the discontinuity in surface curvature and the inherent local pressure gradients introduce length scales to the thin layer of oscillating vorticity imposed by the long-wavelength freestream disturbances. This leads to the development of a TS wave in the boundary layer and its propagation downstream.

The magnitude of total receptivity (measured after the leading-edge-flat-plate juncture) depends on the leading-edge radius of curvature, with sharper leading edges being less receptive to plane parallel sound waves. This is not in conflict with the results of Hammerton and Kerschen (1991) (based on a parabolic body) since the nose radius r_n considered here is relatively large so that contribution from nose bluntness alone will be very small. Hence effects of change of curvature and adverse pressure gradient near the ellipse-flat-plate juncture will dominate the total disturbance response. The contribution from the discontinuity in curvature to receptivity is found to be substantial, making up almost 50 percent of the total receptivity for the AR=6 leading edge at $F=230 \times 10^{-6}$. A new leading-edge geometry for flat plates, based on a modified super ellipse, is proposed to eliminate discontinuous curvature as a source of receptivity so that we can

concentrate on the effects of continuous leading-edge curvature and the associated adverse pressure gradient.

References

Fasel, H. F. 1976 'Investigation of the stability of boundary layers by a finite difference model of the Navier-Stokes equations', J. Fluid Mech. 78, 355-383.

Gatski, T. B. and Grosch, C. E. 1987 'Numerical experiments in boundary-layer receptivity', Proc. Symp. on the Stability of Time Dependent and Spatially Varying Flows, Springer-Verlag, 82-96.

Goldstein, M. E. 1983 'The evolution of Tollmien-Schlichting waves near a leading edge', J. Fluid Mech. 127, 59-81.

Goldstein, M. E. 1985 'Scattering of acoustic waves into Tollmien-Schlichting waves by small streamwise variations in surface geometry', J. Fluid Mech. 154, 509-530.

Goldstein, M. E. and Hultgren, L. S. 1989 'Boundary-layer receptivity to long-wave freestream disturbances', Ann. Rev. Fluid Mech. 21, 137-166.

Hammerton, P. W. and Kerschen, E. J. 1991 'The effect of nose bluntness on leading-edge receptivity', Bull. of the American Physical Society, Vol. 36, No. 10, 2618.

Kachanov, Yu. S., Kozlov, V. V., Levchenko, V. Ya. and Maksimov, V. P. 1978 'The transformation of external disturbances into the boundary layer waves' Proc. Sixth Intl. Conf. on Numerical Methods in Fluid Dynamics (ed. H. Cabannes, M. Holt and V. Rusanov), SpringerVerlag, 299-307.

Kerschen, E. J. 1990 'Boundary layer receptivity theory', Appl. Mech. Rev. vol. 43, no. 5, part 2, S152-157.

Leehey, P. and Shapiro, P. 1980 'Leading-edge effect in laminar boundary layer excitation by sound', Proc. IUTAM Symp. on Laminar-Turbulent Transition, Springer-Verlag, 321-331.

Leehey, P., Gedney, C. J. and Her, J. Y. 1984 'The receptivity of a laminar boundary layer to external disturbances', Proc. IUTAM Symp. on Laminar-Turbulent Transition, Springer-Verlag, 232-242.

Lin, N. 1989 'Receptivity of the boundary layer on a semi-infinite flat plate with an elliptic leading edge', M. S. Thesis, Arizona State University.

Lin, N., Reed, H. L. and Saric W. S. 1991 'Leading-edge receptivity: Navier-Stokes Simulations' Proc. Boundary Layer Transition and Control Conference, Cambridge, U. K.

Morkovin, M. V. 1978 'Instability, transition to turbulence and predictability', AGARDograph No. 236.

Murdock, J. W. 1980 'The generation of Tollmien-Schlichting wave by a sound wave', Proc. Roy. Soc. Lond. A 372, 517-534.

Murdock, J. W. 1981 'Tollmien-Schlichting waves generated by unsteady flow over parabolic cylinders', AIAA paper 81-0199.

Nishioka, M. and Morkovin, M. V. 1986 'Boundary-layer receptivity to unsteady pressure gradients: Experiments and overview', J. Fluid Mech. 171, 219-261.

Parekh, D. E., Pulvin, P. and Wlezien, R. W. 1991 'Boundary layer receptivity to convected gust and sound', Proc. 1st ASME-JSME Fluids Engineering Conference, Portland, OR.

Reshotko, E. 1984 'Environment and receptivity', AGARD Report No. 709 (Special course on stability and transition of laminar flows) VKI, Brussels.

Schneider, G. E. and Zedan, M. 1981 'A modified strongly implicit procedure for the numerical solution of field problems', Numerical Heat Transfer, 4, 1-19.

Wlezien, R. W. and Parekh, D. E. 1990 'Measurement of acoustic receptivity at leading edges and porous strips', Bull. of the American Physical Society, Vol. 35, No. 10, 2262.
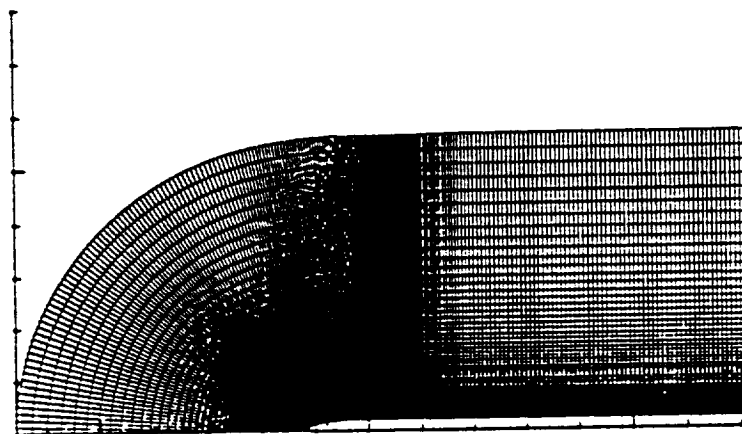
Figure 1. Generated C-type grid; AR=6, Re=2400.
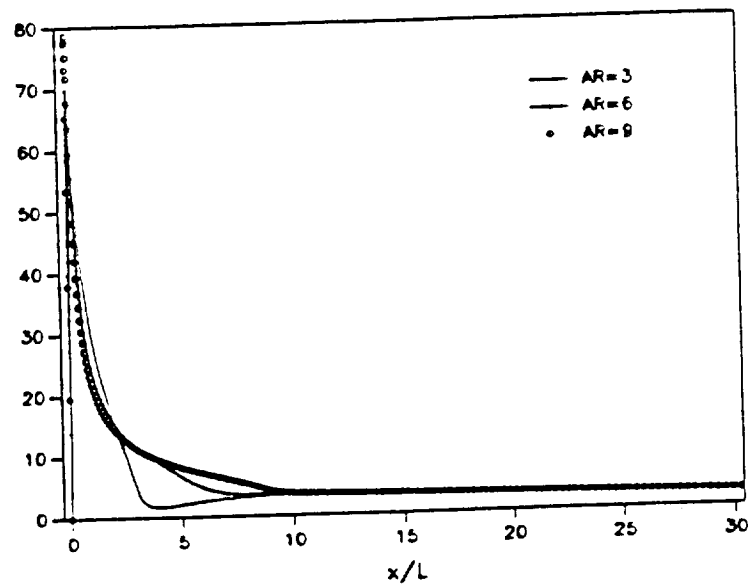
Figure 2. Steady-state vorticity distribution along the wall; Re=2400.
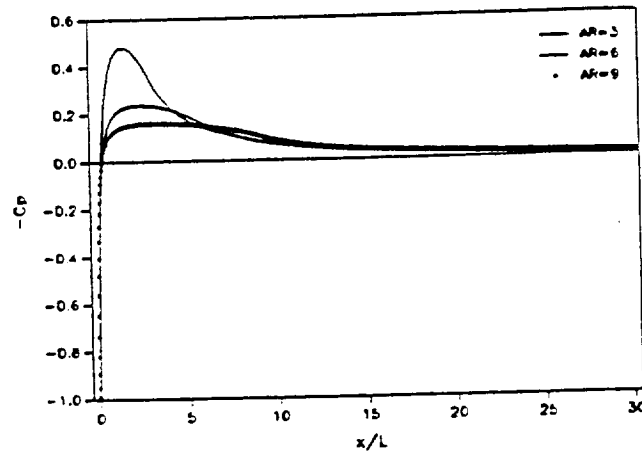
Figure 3. Surface pressure coefficient Cp; Re=2400.
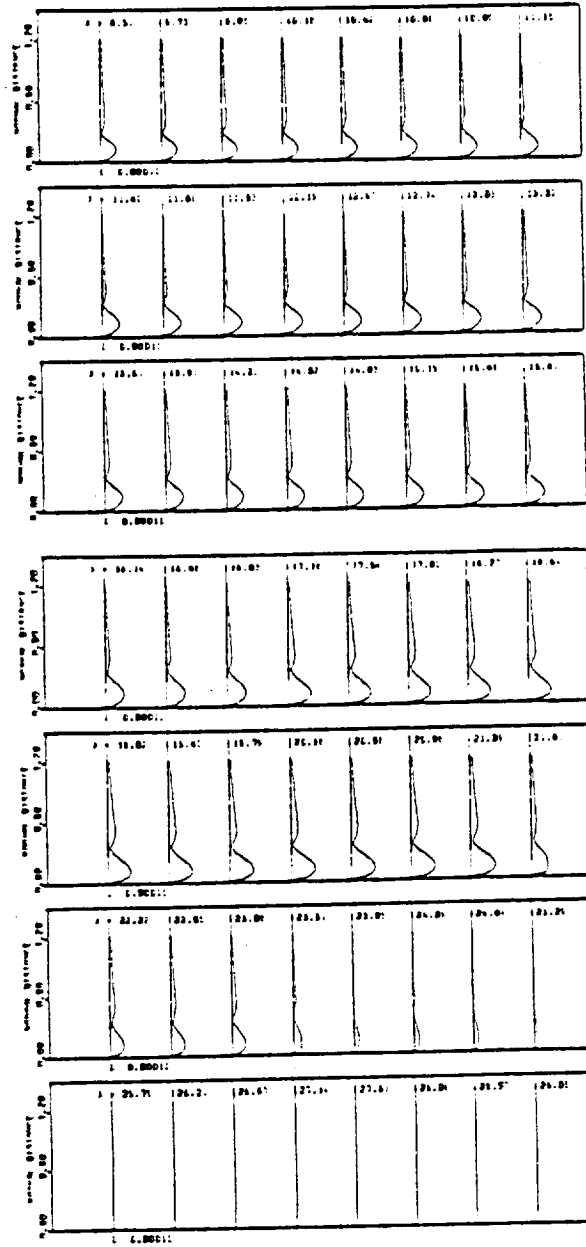
Figure 4. Amplitude profiles of u'/U taken during the fourth cycle at consecutive downstream locations, after the Stokes wave is subtracted; AR=3, F=230x10⁻⁶, a/U=10⁻⁴ .
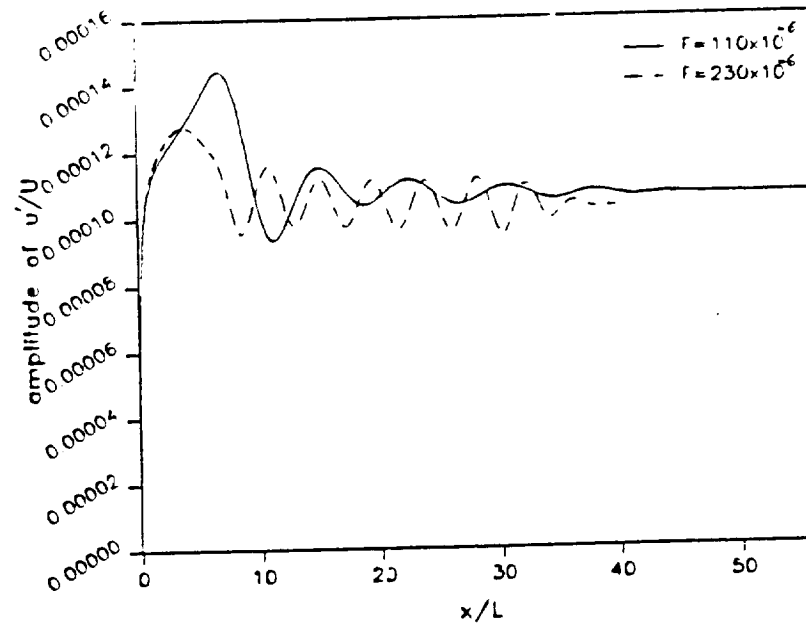
Figure 5. Amplitude of streamwise disturbance velocity, u'/U vs. x; AR=6, Re=2400.
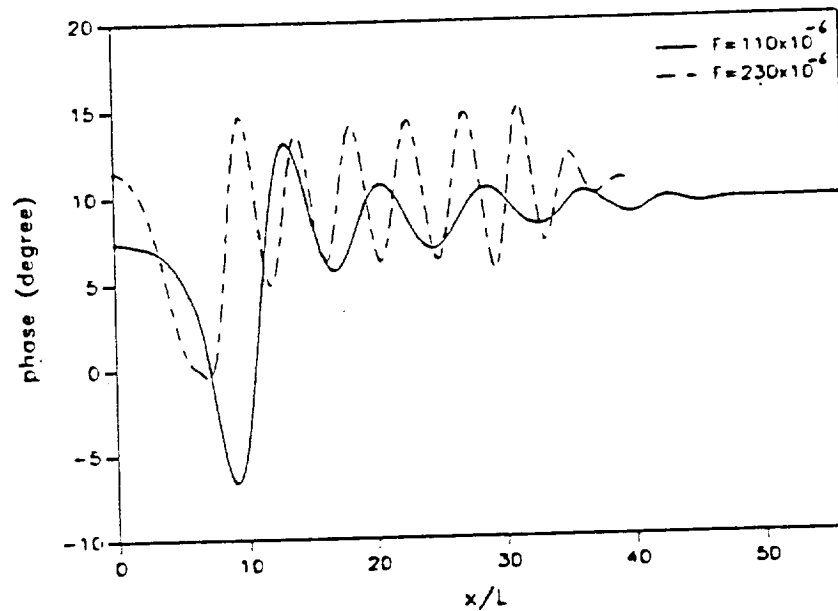
Figure 6. Phase of streamwise disturbance velocity, u'/U vs. x; AR=6, Re=2400.
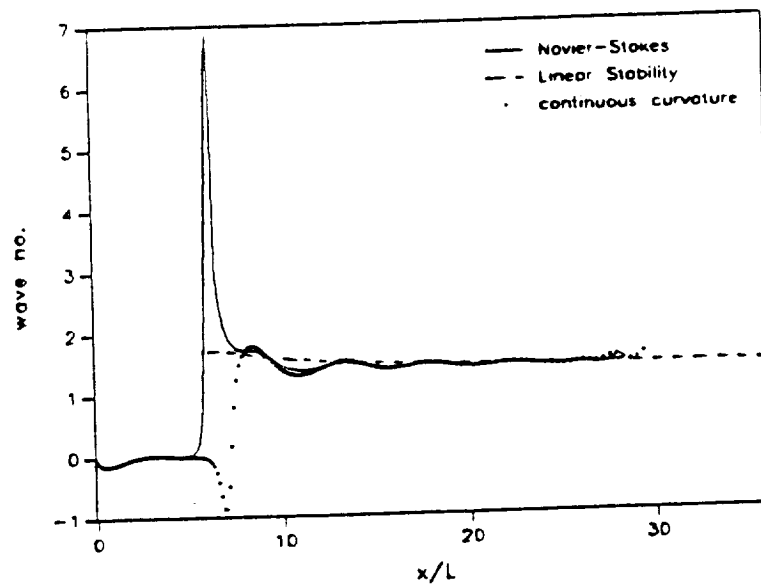
Figure 7. Variation of wave number α L (of v') vs. x, taken after 6
cycles; AR=6, F=230x10^{-6}.
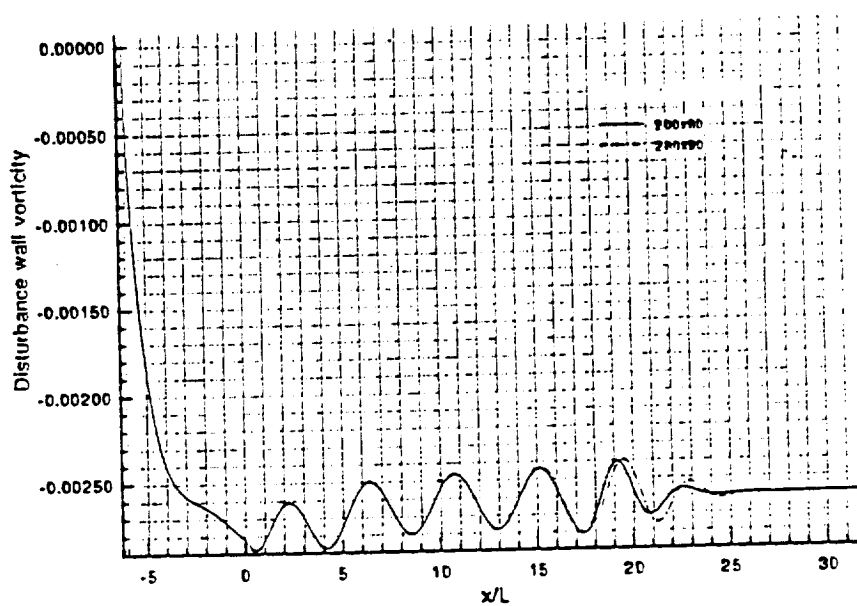
Figure 8. Instantaneous disturbance wall vorticity ω'L/U obtained
with two different grid resolutions after 4 cycles of forcing;
AR=6, F=230x10^{-6}, a/U=10^{-4}.
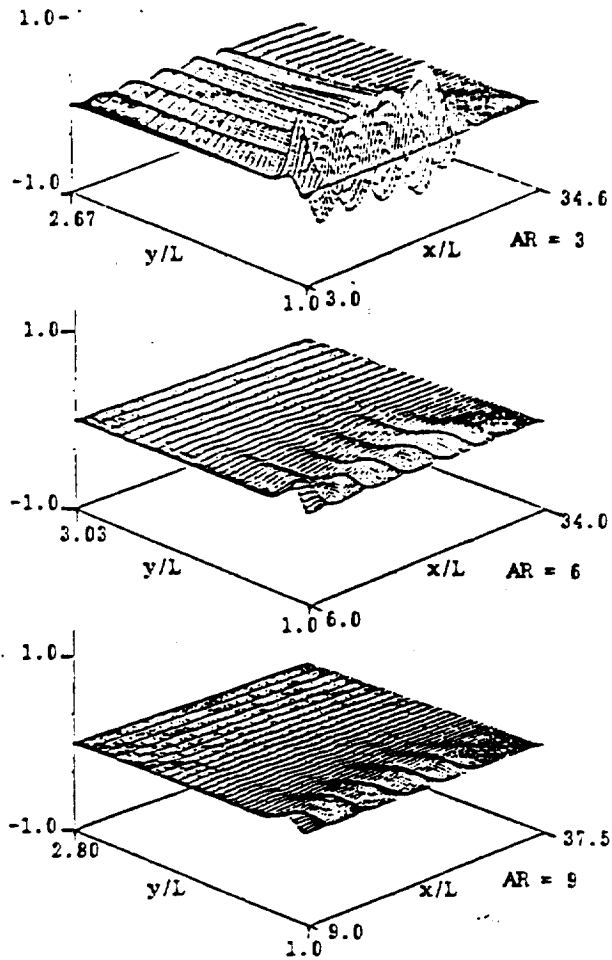
Figure 9. Surface plots of u'/a after 4 cycles of forcing, after the Stokes wave is subtracted; $F=230\times10^{-6}$, AR=3, 6 and 9.
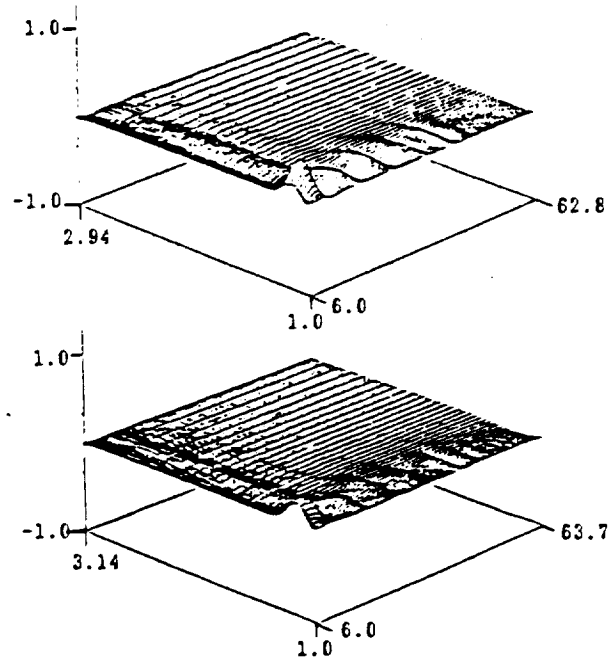
Figure 10. Surface plots of u'/a after 4 cycles of forcing, after the Stokes wave is subtracted; $F=110\times10^{-6}$, AR= 6 and 9.
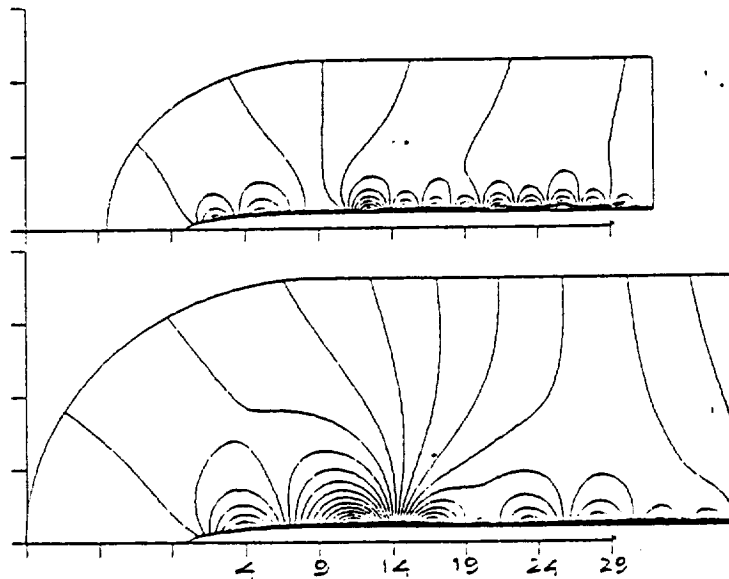
Figure 11. Contours of instantaneous disturbance streamlines after 4 cycles of forcing; AR=9, $F=230\times10^{-6}$ and 110×10^{-6}..
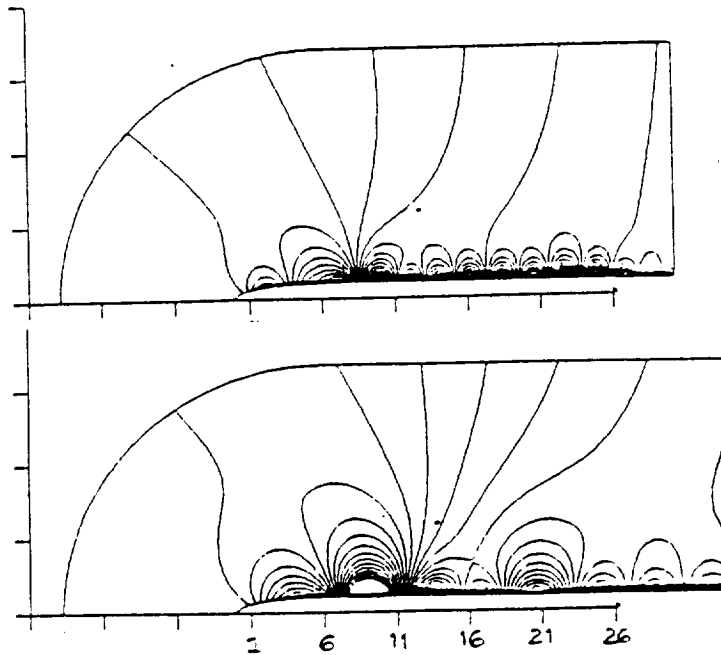
Figure 12.a. Contours of instantaneous disturbance streamlines after 4 cycles of forcing; AR=6, F=230x10^{-6} and 110x10^{-6}..
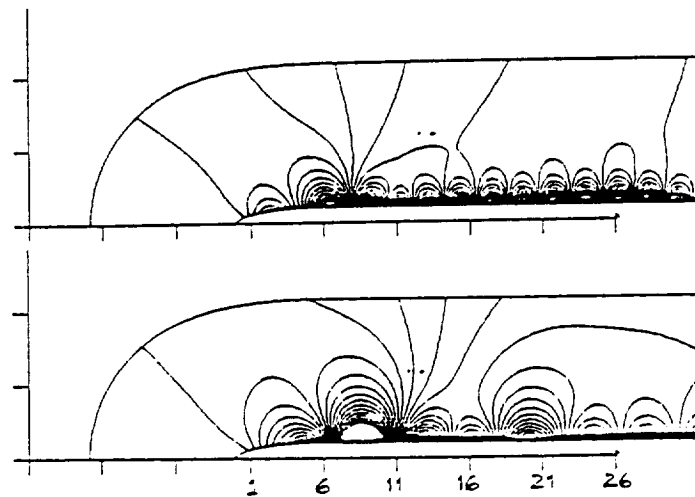
Figure 12.b. Contours of instantaneous disturbance streamlines after 5 cycles at F=230x10^{-6} and after 4 cycles at F=110x10^{-6}; MSE, AR=6.
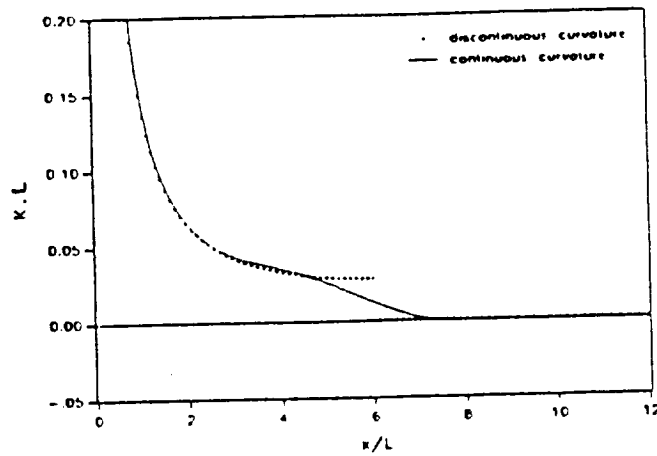
Figure 13. Variation of curvature of the AR=6 leading edge near the juncture.

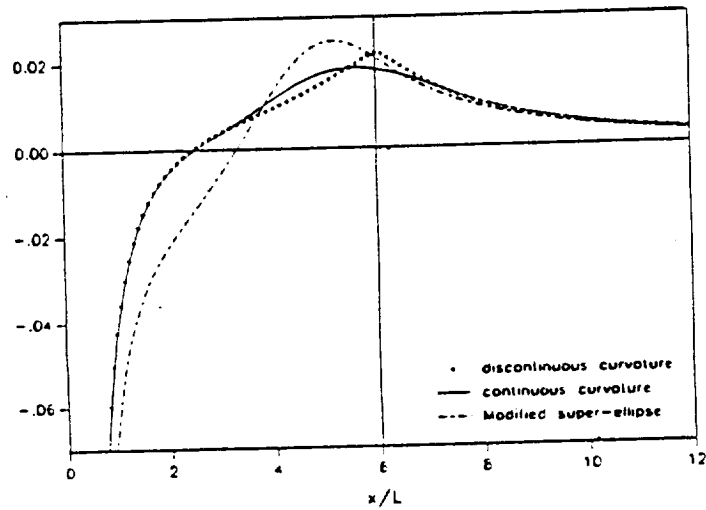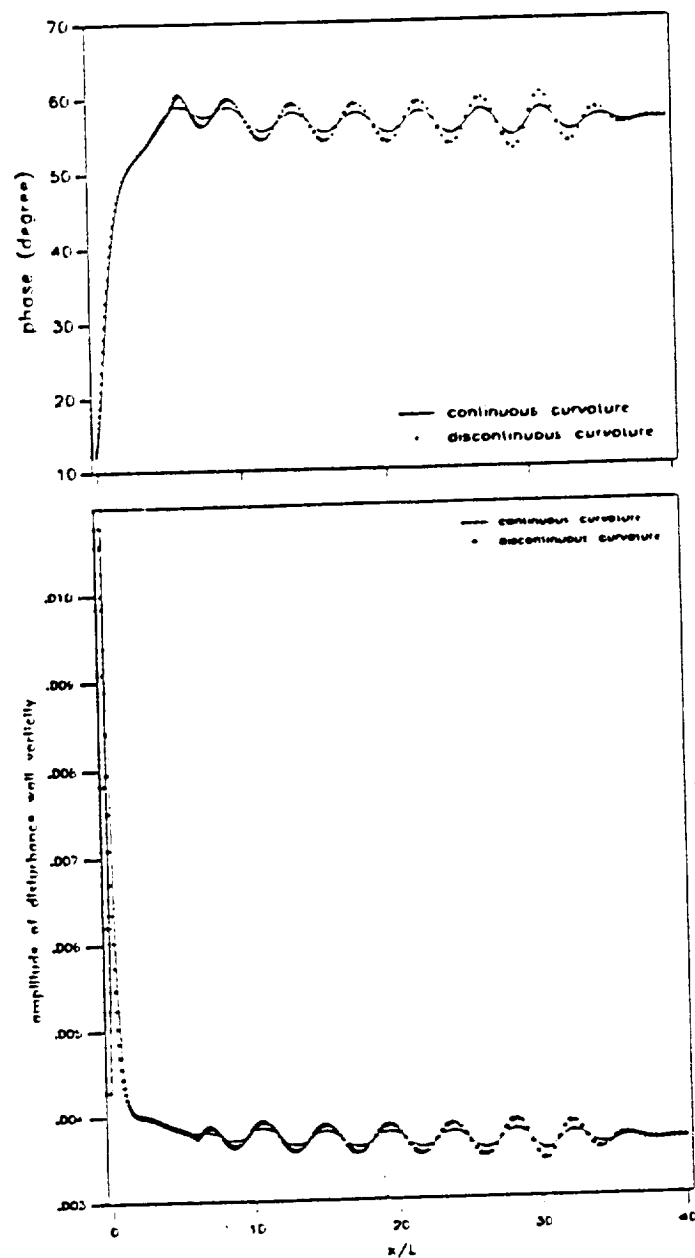Figure 14. Enlarged view of the steady pressure gradient along the surface, near the juncture; AR=6, Re=2400.

Figure 15. Amplitude and phase of disturbance wall vorticity ω'L/U taken after 6 cycles of forcing; AR=6, F=230x10⁻⁶, a/U= 10⁻⁴.
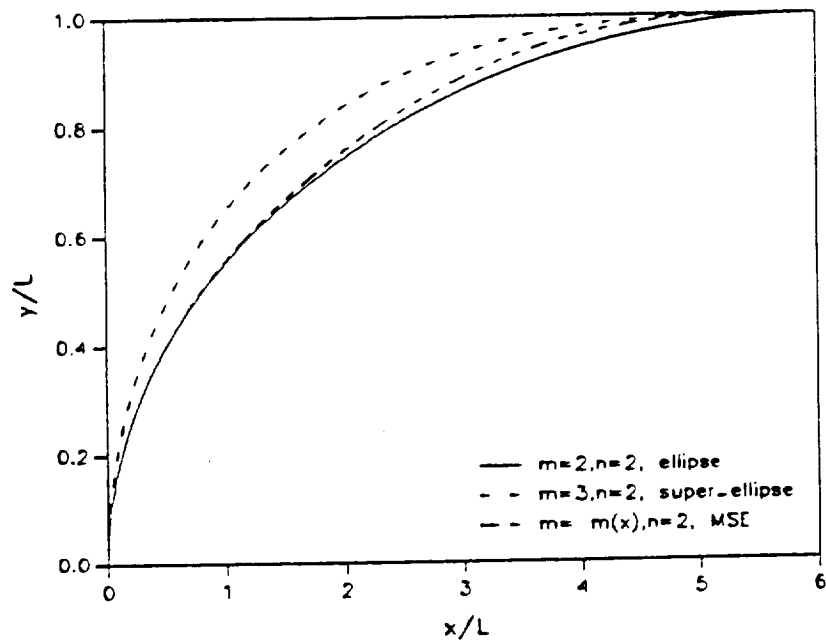
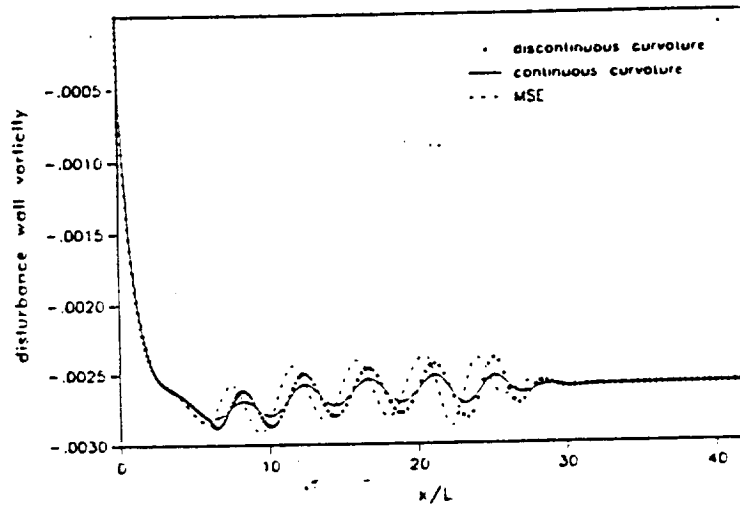Figure 16. Shapes of the super-ellipse with m=3, n=2 and the modified super-ellipse, AR=6.

Figure 17. Instantaneous disturbance vorticity $\omega'L/U$ along the wall, after 4 cycles of forcing; AR=6, F=230x10^{-6}, a/U= 10^{-4}.